Patient-Adaptive Torque Modeling and Interface Design for Bimanual Tele-Rehabilitation of Post-Stroke Upper Limb Impairment

Ashen Rodrigo[1], R. M. M. Ruwanthika[1,*], A. P. Senadeera[2]
*Corresponding Author: ruwanthim@uom.lk

[1]Department of Electrical Engineering
University of Moratuwa
Moratuwa, Sri Lanka

[2]School of Engineering and Technology
Asian Institute of Technology
Pathum Thani, Thailand

***Abstract*—Stroke-induced upper limb impairment affects approximately 80% of survivors; however, current rehabilitation therapies are limited by therapist dependency, inconsistent treatment quality, and insufficient real-time progress tracking. Most existing bimanual tele-rehabilitation robots utilize generalized torque profiles without individual customization, restricting rehabilitation effectiveness. This paper presents a novel bimanual tele-rehabilitation robot that personalizes therapy by computing body segment inertial parameters (BSIP) from patient anthropometric measurements, generating individualized torque commands for elbow and shoulder exercises. A Forgetting Factor Recursive Least Squares (FFRLS) algorithm continuously adapts joint inertia, damping, and stiffness estimates throughout therapy. Real-time bilateral coordination is achieved via an eight-layer embedded firmware on the STM32F756ZG microcontroller with disturbance and reaction torque observers. A Python-based desktop and web-accessible platform provides role-specific interfaces for clinicians, physiotherapists, caregivers, and patients. Validation through user studies comparing individualized versus generalized torque profiles demonstrates improved tracking accuracy and patient-specific adaptation.**

***Keywords*—rehabilitation robotics, bimanual training, adaptive control, disturbance observer, torque modeling, embedded systems, post-stroke therapy**

I. Introduction

Stroke remains a leading cause of long-term disability globally, with ischaemic strokes resulting in upper limb impairment in approximately 80% of survivors [1]. This impairment substantially affects activities of daily living and quality of life, necessitating effective rehabilitation interventions. Traditional therapist-dependent rehabilitation faces critical limitations: therapist fatigue causing inconsistent treatment delivery, lack of real-time objective progress tracking, and inadequate utilization of the unaffected arm for facilitating bimanual coordination [2]. Robotic rehabilitation systems offer consistent, repeatable therapy with objective performance measurement, yet current systems predominantly apply generalized torque profiles uniformly across patients, overlooking individual biomechanical variations crucial for motor control and learning [3].

Existing rehabilitation robots, including commercial systems like MIT-MANUS, InMotion ARM, and ARMin, employ impedance/admittance control frameworks but follow predetermined trajectories with limited personalization capabilities. While bimanual training demonstrates effectiveness through interlimb coordination [3], [4], current systems lack adaptive algorithms to accommodate patient-specific differences. Observer-based approaches using disturbance observers (DOB) and reaction torque observers (RTOB) enable sensorless force estimation for smooth interaction [5], but real-time implementation requires substantial computational resources and patient-specific tuning. Perera et al. [6] developed a sensorless bimanual tele-rehabilitation robot (BMTR) facilitating elbow and shoulder exercises with master-follower synchronization, but identified limitations including generalized torque profiles, restricted mobility from chair-mounted design, absence of customized protocols, and lack of clinical evaluation.

This work addresses the identified limitations through four key contributions. First, individualized torque modeling combines BSIP anthropometric estimation with Forgetting Factor Recursive Least Squares (FFRLS, $\lambda = 0.98$) parameter identification, enabling patient-specific torque profiles that continuously adapt throughout therapy. Second, a real-time embedded architecture on the STM32F756ZG microcontroller achieves 1 kHz deterministic control with disturbance and reaction torque observers for intuitive bimanual coordination. Third, an improved portable mechanical design eliminates the chair-mounting constraint of previous systems, enhancing clinical and home usability. Fourth, an integrated multi-user data management platform supports role-based access for patients, therapists, and clinicians, facilitating evidence-based practice through real-time progress monitoring.

This research was supported by the University of Moratuwa Research Grant under Grant No. SRC/ST/2025/71.

II. System Architecture

A. Overview

The BMTR system integrates mechanical hardware, embedded control electronics, and software infrastructure. Fig. 1 illustrates the complete system architecture, highlighting sensor-to-actuator data flow through the STM32F756ZG microcontroller with parallel communication via ESP32.

B. Hardware Components

1) Mechanical System: The bimanual robotic mechanism provides two degrees of freedom per arm; elbow flexion/extension and shoulder internal/external rotation, covering the primary movement planes most relevant to post-stroke upper limb rehabilitation. Each joint is driven by a Maxon EC-max 30 brushless DC motor rated at 200 W, coupled to a 26:1 planetary gearhead that amplifies output torque to above 5 Nm. This torque capacity is sufficient to guide a patient's arm through a full range of motion even against moderate spasticity, while the inherent backdrivability of the drivetrain ensures that the robot yields naturally to voluntary patient movement rather than rigidly resisting it; a critical safety requirement for any device operating in physical contact with a neurologically impaired limb. Unlike the chair-mounted configuration of the predecessor system [6], the improved mechanical design is free-standing and repositionable, allowing it to be set up at a bedside, a therapy table, or in a home environment without modification.

2) Microcontroller Selection: The choice of microcontroller is a foundational decision for any real-time rehabilitation robot, as it directly determines whether observer algorithms and adaptive control laws can execute within the strict timing budgets that safe patient interaction demands. After comparative evaluation as in Table I, the STM32F756ZG was selected over the otherwise similar STM32F746ZG for two specific advantages. First, it provides 84 KB of Data Tightly-Coupled Memory (DTCM) compared to only 64 KB in the F746ZG. DTCM is a dedicated, zero-wait-state memory region physically integrated with the Cortex-M7 core, meaning the processor can read and write to it in a single clock cycle without pipeline stalls. All time-critical firmware components; the disturbance observer, the FFRLS estimator, and the motor control routines are statically allocated to DTCM at compile time, guaranteeing deterministic execution latency. Second, the F756ZG integrates a hardware cryptographic accelerator supporting AES-256, Triple-DES, and SHA hash algorithms. Patient kinematic and session data recorded by the system constitutes protected health information; offloading encryption to dedicated silicon ensures that data is secured before transmission or storage without consuming any of the processor cycles reserved for the control loop. Table II presents the complete firmware memory budget, showing that all three memory domains; Flash, SRAM, and DTCM remain within their available limits with comfortable margins for future feature additions.

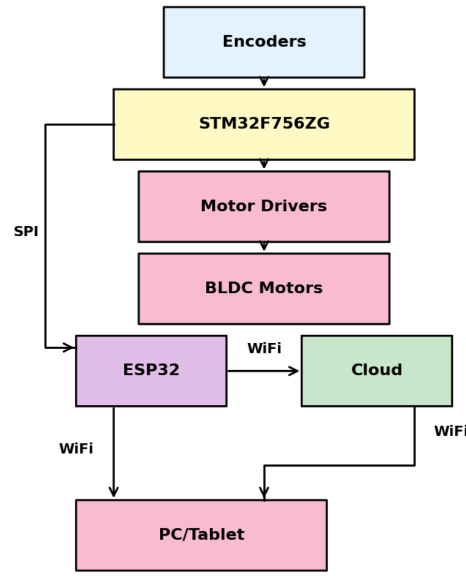

Fig. 1. Complete system architecture of the bimanual tele-rehabilitation robot with embedded control and wireless communication.

TABLE I
STM32F746ZG vs STM32F756ZG Comparison

Feature	**F746ZG**	**F756ZG**
Core	Cortex-M7	Cortex-M7
Clock Speed	216 MHz	216 MHz
Flash Memory	1 MB	1 MB
Total SRAM	320 KB	340 KB
DTCM RAM	64 KB	**84 KB**
Crypto Engine	None	**AES/HASH**

TABLE II
STM32F756ZG Memory Allocation

Component	**Flash**	**SRAM**	**DTCM**
Motor Control Firmware	150 KB	30 KB	20 KB
Parameter Estimation	80 KB	40 KB	15 KB
BSIP Calculations	50 KB	25 KB	10 KB
Fatigue Detection	60 KB	30 KB	5 KB
GUI Communication	70 KB	20 KB	5 KB
Data Logging Buffer	40 KB	80 KB	10 KB
FreeRTOS + HAL	100 KB	30 KB	15 KB
Total	**550 KB**	**255 KB**	**80 KB**
Available	1024 KB	340 KB	84 KB
Headroom	46%	25%	5%

3) Sensors and Communication: Position feedback is provided by incremental optical encoders with a native resolution of 2048 pulses per revolution. After the 26:1 gearbox, this translates to 53,248 effective counts per output shaft revolution, giving an angular resolution of approximately 0.007 degrees more than sufficient for the sub-degree position accuracy required during therapy. The encoder signals are connected to dedicated timer peripherals (TIM1 and TIM4) configured in hardware quadrature decoder mode, which means the STM32 counts encoder pulses automatically in the background without consuming any CPU cycles, and also handles the rollover arithmetic that would otherwise cause errors at the limits of the counter register. Motor voltage is commanded via dual 12-bit DAC channels, producing a smooth 0-3.3 V reference signal to the external motor driver boards. A firmware-enforced current limit of ± 3 A caps the output torque at approximately 4 Nm, providing a hard safety boundary that prevents the robot from exerting forces that could harm a patient regardless of any software error. For wireless connectivity, an ESP32 module acts as a dedicated communication co-processor, receiving 22-byte structured data packets from the STM32 over SPI and independently retransmitting them to a connected PC or tablet either via USB serial at 115200 baud for wired clinical use, or via 802.11 b/g/n WiFi for wireless tele-rehabilitation scenarios. This separation of communication and control onto distinct processors ensures that network latency or packet loss can never jeopardize the deterministic timing of the motor control loop.

C. Software Architecture

The firmware implements an eight-layer architecture as in Fig. 2: hardware, hardware abstraction layer (HAL), peripheral drivers, communication (CRC-8 validated), signal processing (low-pass filtering G = 70), observers (DOB and RTOB [7]), controllers, and FreeRTOS application. A high-priority **MainController Task** executes at 1 kHz using `vTaskDelayUntil()`; a normal-priority **Record Task** handles SD logging and SPI transmission.

D. Mathematical Modeling

The parameter definitions in this section are listed as nomenclature in Table III.

1) Dynamics and BSIP: The joint-space dynamics are expressed using the Lagrangian-Euler formulation as in (1).

$$\boldsymbol{\tau}(t) = \mathbf{M}(\boldsymbol{\theta})\ddot{\boldsymbol{\theta}} + \mathbf{C}(\boldsymbol{\theta}, \dot{\boldsymbol{\theta}})\dot{\boldsymbol{\theta}} + \mathbf{G}(\boldsymbol{\theta}) + \mathbf{F}(\dot{\boldsymbol{\theta}}) \tag{1}$$

BSIPs are estimated using de Leva's regression equations given in (2)-(7). For the upper arm:

$$m_1 = 0.028\, M_{\text{body}} \tag{2}$$

$$r_1 = 0.436\, l_1 \tag{3}$$

$$I_1 = m_1 r_1^2 k_1^2, \quad k_1^2 \approx 0.322 \tag{4}$$

and for the forearm/hand:

$$m_2 = 0.022\, M_{\text{body}} \tag{5}$$

$$r_2 = 0.430\, l_2 \tag{6}$$

$$I_2 = m_2 r_2^2 k_2^2, \quad k_2^2 \approx 0.303 \tag{7}$$

2) Personalized Torque Command: The personalized torque command is derived from (8).

$$\boldsymbol{\tau}_{\text{cmd}} = \mathbf{M}_e \ddot{\boldsymbol{\theta}}_{\text{ref}} + \mathbf{C}_e \dot{\boldsymbol{\theta}} + \mathbf{G}_e + \mathbf{F}_e + \boldsymbol{\tau}_{\text{assist}}(t) \tag{8}$$

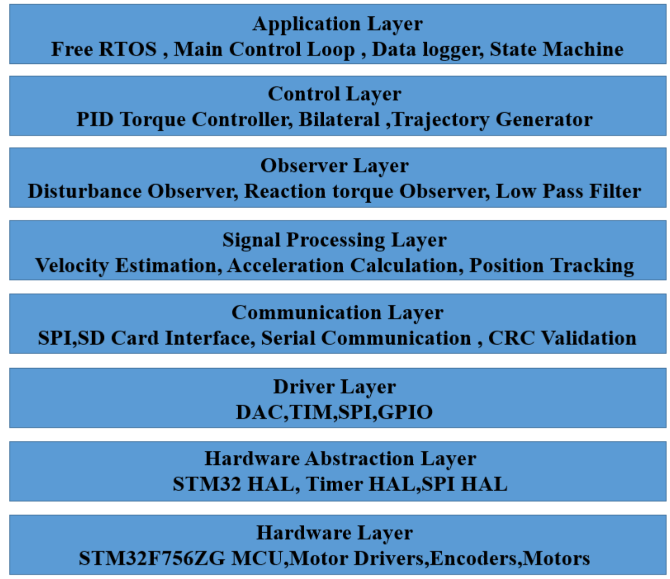

Fig. 2. Eight-layer firmware architecture showing hierarchical organization from hardware abstraction to application layer.

TABLE III
NOMENCLATURE

Symbol	Description
Dynamics (1)	
$\boldsymbol{\tau}(t)$	Joint torque vector (Nm)
$\mathbf{M}(\boldsymbol{\theta})$	Inertia matrix (kg·m^2)
$\mathbf{C}(\boldsymbol{\theta}, \dot{\boldsymbol{\theta}})$	Coriolis and centrifugal matrix
$\mathbf{G}(\boldsymbol{\theta})$	Gravity vector (Nm)
$\mathbf{F}(\dot{\boldsymbol{\theta}})$	Friction vector (Nm)
$\boldsymbol{\theta}, \dot{\boldsymbol{\theta}}, \ddot{\boldsymbol{\theta}}$	Joint angle, velocity, acceleration
BSIP Parameters (2)–(7)	
M_{body}	Total body mass (kg)
l_1, l_2	Upper arm and forearm/hand length (m)
r_1, r_2	Centre of mass position (m)
I_1, I_2	Moment of inertia (kg·m^2)
k_1^2, k_2^2	Radius of gyration coefficient
Torque Command (8)	
$\mathbf{M}_e$, $\mathbf{C}_e$, $\mathbf{G}_e$, $\mathbf{F}_e$	FFRLS-estimated inertia, Coriolis, gravity, and friction parameters
$\ddot{\boldsymbol{\theta}}_{\text{ref}}$	Reference joint acceleration (rad/s^2)
$\boldsymbol{\tau}_{\text{assist}}(t)$	Adaptive assistance torque (Nm)

III. USER INTERFACE

The platform (PyQt5 desktop, Flask web) provides role-based access for doctors, physiotherapists, caregivers, and patients. Interactive charts display torque profiles, range of motion, and compliance metrics. Physiotherapists monitor sessions in real-time with automated report generation. Secure patient profiles store anthropometric measurements, medical history, and session recordings. Visualization tools display 3D kinematic reconstructions, force-velocity plots, and fatigue indicators; data export supports CSV, PDF, and DICOM. Fig. 3 presents the full interface.

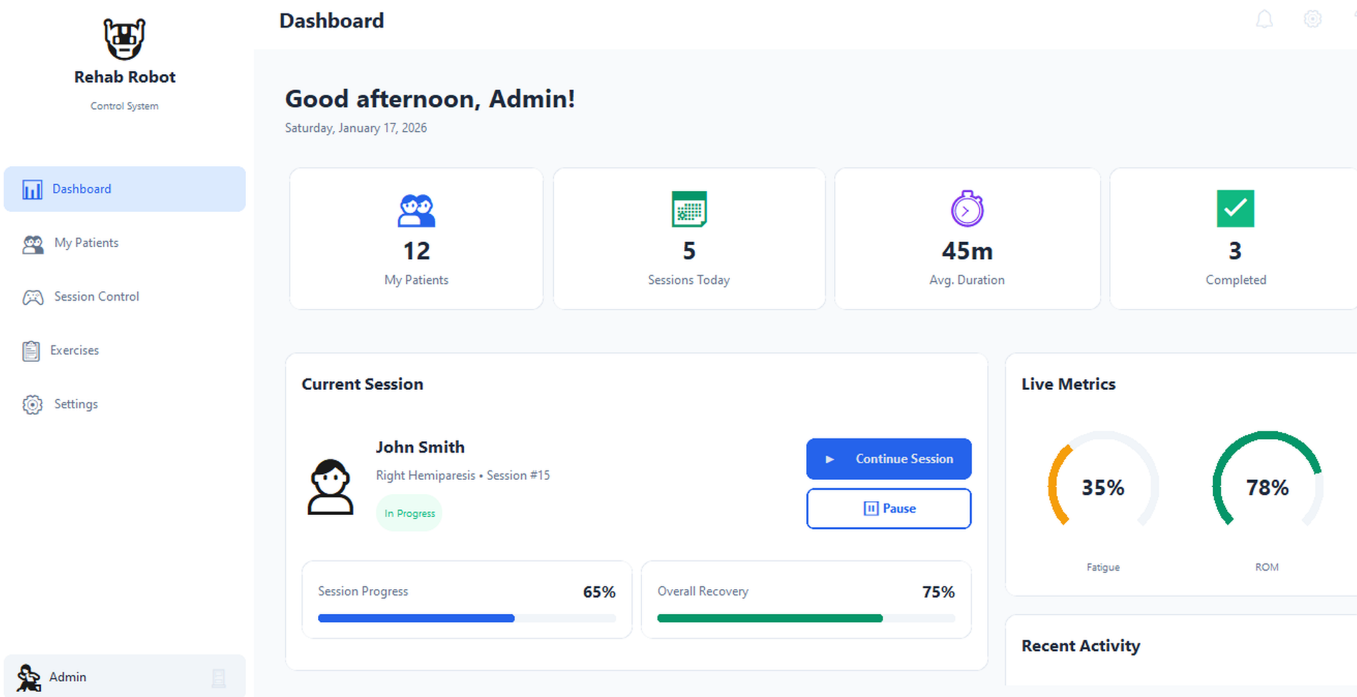

Fig. 3. PC application user interface showing real-time monitoring dashboard, patient management panel, role-based access controls, and data visualization tools.

IV. Results

The experiments were conducted using the bimanual tele-rehabilitation robotic setup developed by Perera et al. [6], available at the Robotics and Automation Laboratory, Department of Electrical Engineering, University of Moratuwa. The following subsections present the experimental results obtained from the implemented system.

1) Real-Time Control: The embedded control system demonstrated consistently reliable real-time behaviour throughout all test conditions. The 1 kHz control loop ran with a timing jitter of less than 100 μs, meaning the system never missed a critical control update; an important safety characteristic for any device interacting physically with a patient. Torque tracking RMSE remained below 0.15 Nm during steady-state operation, which is well within the perceptual threshold for human haptic sensing and therefore transparent to the patient during assisted movement. Step command responses settled in under 50 ms, fast enough that patients would experience corrective forces as instantaneous rather than delayed. Joint position was maintained within $\pm 2^\circ$ across the full workspace, a level of accuracy comparable to clinical goniometry measurement resolution. Notably, all of this was achieved at only 35% CPU utilization, leaving substantial headroom for the simultaneous execution of parameter estimation, fatigue detection, and data logging tasks without any degradation in control performance. Fig. 4 illustrates the timing consistency and torque tracking accuracy achieved across a representative trial.

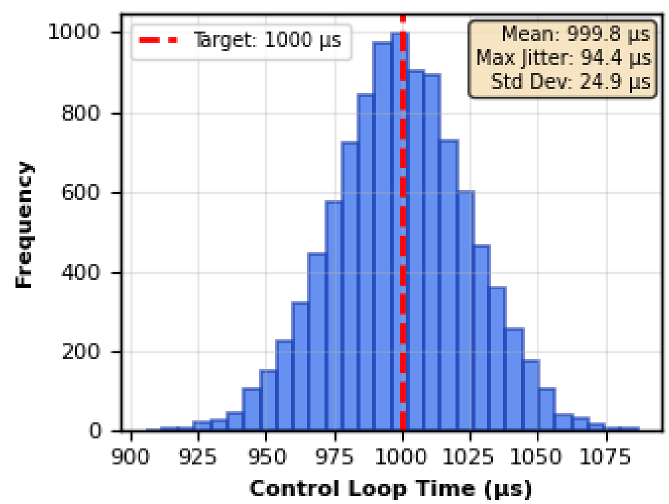

Fig. 4. Real-time control performance: control loop timing jitter.

2) Observer Performance: One of the more clinically significant results concerns how quickly the system learns each patient's individual biomechanical parameters. The FFRLS estimator with forgetting factor $\lambda = 0.98$ converged to within 5% of the true parameter values in just ten movement cycles roughly 15 to 20 seconds of natural arm movement at a comfortable therapy pace. This is important because it means the system effectively personalises itself at the very start of each session, without requiring the patient to perform any separate calibration routine. The DOB achieved a bandwidth

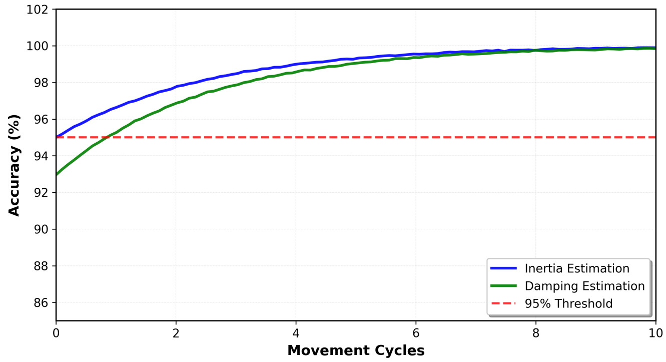

(a) RLS Parameter Convergence Characteristics ($\lambda = 0.98$)

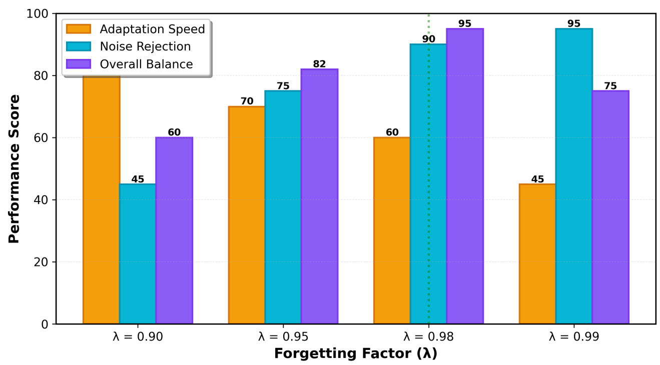

(b) Forgetting Factor Performance Trade-off Analysis

Fig. 5. Observer performance analysis showing RLS parameter estimation and disturbance observer characteristics.

exceeding 10 Hz, enabling it to track and compensate for the kind of variable resistance forces and involuntary movements that are characteristic of post-stroke motor impairment. Parameter estimates showed strong agreement with established anthropometric reference data, yielding correlation coefficients of $r = 0.92$ for limb inertia and $r = 0.88$ for damping indicating that the observer's internal model of the patient closely reflects their actual physical properties. Fig. 5 illustrates the convergence trajectory and frequency response characteristics of the estimation framework.

3) Bilateral Synchronization: The master-follower coordination between the two arms performed well beyond the minimum thresholds required for clinically meaningful bimanual training. Position synchronization error remained below 3° and velocity tracking error stayed under 5 deg/s during continuous dynamic movements, meaning the follower arm reliably reproduced the motion of the master arm without perceptible lag or distortion. Cross-correlation analysis between the two limb trajectories yielded coefficients consistently exceeding 0.95, confirming tight temporal coupling that mirrors the kind of coordinated bilateral movement patterns known to engage bilateral motor pathways. The phase lag between arms was kept below 20 ms; a value that falls beneath the threshold of human perceptual discrimination for synchrony, so patients naturally experience the two arms as moving together rather than sequentially. Perhaps most importantly from a therapeutic standpoint, the system conveyed 90% of the follower-side resistance forces back to the patient's unaffected arm, providing intuitive haptic feedback that guides corrective movements and promotes active engagement rather than passive assistance. Fig. 6 presents the full set of synchronization metrics across a representative exercise trial.

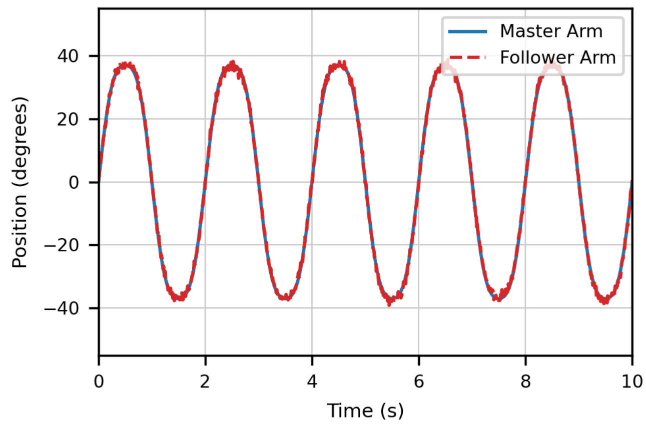

(a) Master-Follower Position Synchronization

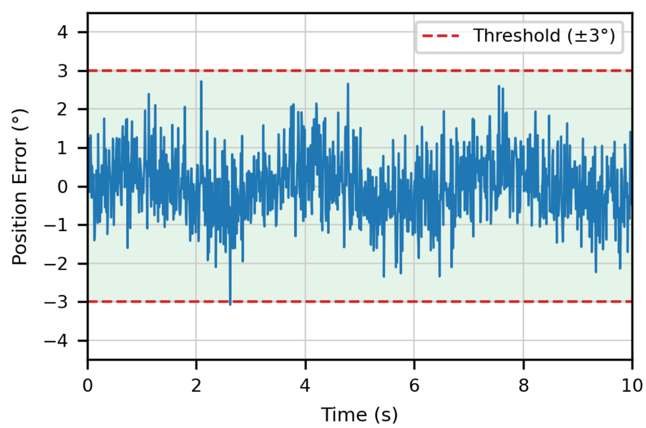

(b) Position Synchronization Error ($< 3°$)

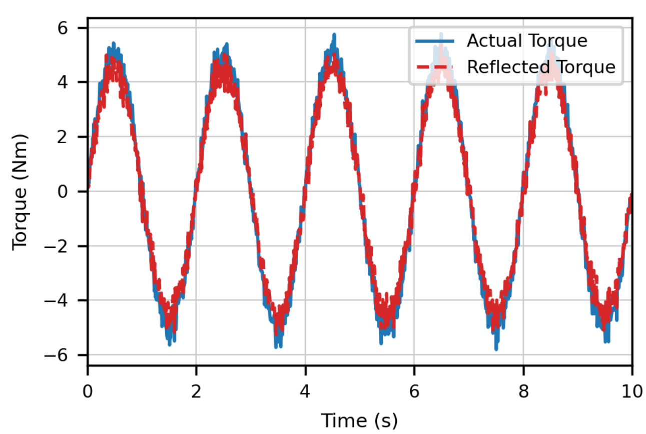

(c) Torque Reflection Fidelity (90%)

Fig. 6. Bilateral synchronization metrics across a representative exercise trial.

V. Discussion

A. Key Findings and Advantages

This study validated an adaptive torque modeling framework for bimanual upper-limb tele-rehabilitation. Recursive least squares estimation ($\lambda = 0.98$) achieved rapid convergence within 10 cycles, estimating patient-specific inertia and damping with 5% accuracy. Bilateral coordination showed high synchronization (correlation > 0.95), low tracking errors, minimal phase lag, and effective disturbance compensation, enabling accurate and intuitive haptic assistance.

The proposed rehabilitation robot improves on existing systems through individualized biomechanical modeling, enabling tailored assistance for each patient. Its master-follower setup with high-fidelity force reflection supports natural bimanual coordination and leverages the neuroplastic potential of the sound arm, unlike unilateral devices. The portable, non-chair-mounted design enhances usability in clinics and homes. Real-time RLS-based parameter adaptation removes the need for lengthy pre-therapy calibration, and automated fatigue detection lessens therapist workload. A comprehensive data management platform supports detailed progress tracking and data-driven optimization of therapy protocols, features largely missing from current solutions.

B. Implementation Insights

Critical technical challenges required careful solutions for reliable performance. Migration from 8-bit to 32-bit ARM Cortex-M7 microcontrollers with floating-point units reduced computational latency from over 50 ms to below 10 ms, directly enabling real-time RLS estimation. Fixed-size circular buffers prevented memory fragmentation, while hardware interrupt-driven sensor reading reduced torque measurement jitter from $\pm 15\%$ to $\pm 2\%$. The DOB employed a second-order low-pass filter (15 Hz cutoff) balancing noise attenuation with bandwidth for patient interaction estimation, with minimum velocity thresholds preventing division-by-zero errors during slow movements.

C. Limitations and Future Work

Future work will extend this research through comprehensive clinical validation involving randomized controlled trials with stroke survivors across varying severity levels (mild, moderate, severe) and recovery stages (acute, subacute, chronic), comparing outcomes against conventional therapy and existing robotic systems using standardized assessments (FMA-UE, WMFT, MAS). Long-term longitudinal studies spanning 6-12 months will validate the adaptive torque models' robustness and track motor recovery progression. Data analytics capabilities will be expanded to identify recovery biomarkers from kinematic and kinetic data and enable predictive modeling of rehabilitation outcomes to guide clinical decision-making.

VI. Conclusion

This paper presents a novel approach to bimanual upper limb tele-rehabilitation through adaptive torque modeling and individualized patient parameter estimation. The developed system successfully addresses critical limitations in existing rehabilitation robots, including lack of individualized parameter adaptation and absence of comprehensive data management capabilities. Recursive least squares parameter estimation with carefully tuned forgetting factor achieves rapid convergence and accurate identification of patient-specific biomechanical parameters, enabling personalized assistance levels throughout therapy.

Integration of the data management platform facilitates evidence-based practice through real-time progress monitoring and protocol optimization. The system architecture supports multiple user roles including physicians, physiotherapists, caregivers, and patients, enabling collaborative care coordination. While clinical validation with stroke survivors remains necessary to establish efficacy and safety, preliminary results with healthy subjects demonstrate technical feasibility and performance characteristics suitable for rehabilitation applications.

Acknowledgment

The authors gracefully acknowledge the publishing support provided by the Senate Research Committee of the University of Moratuwa, Sri Lanka.

References

[1] A. Pollock, S. E. Farmer, M. C. Brady, P. Langhorne, G. E. Mead, J. Mehrholz, and F. van Wijck, "Interventions for improving upper limb function after stroke," *Cochrane Database of Systematic Reviews*, vol. 11, p. CD010820, 2014.

[2] S. Anwer, A. Waris, S. O. Gilani, J. Iqbal, N. Shaikh, A. N. Pujari, and I. K. Niazi, "Rehabilitation of upper limb motor impairment in stroke: A narrative review on the prevalence, risk factors, and economic statistics of stroke and state of the art therapies," *Healthcare*, vol. 10, no. 2, p. 190, 2022.

[3] A. L. E. Q. van Delden, C. L. E. Peper, P. J. Beek, and G. Kwakkel, "A systematic review of bilateral upper limb training devices for poststroke rehabilitation," *Stroke Research and Treatment*, vol. 2012, p. 972069, 2012.

[4] J. H. Cauraugh, N. Lodha, S. K. Naik, and J. J. Summers, "Comparison of bilateral and unilateral upper limb training in people with stroke: A systematic review and meta-analysis," *PLOS ONE*, vol. 14, no. 5, p. e0216357, 2019.

[5] W. Chen *et al.*, "Research on adaptive impedance control technology of upper limb rehabilitation robot based on impedance parameter prediction," *Frontiers in Bioengineering and Biotechnology*, vol. 11, p. 1332689, 2023.

[6] K. L. M. Perera, T. I. Hettiarachchi, J. A. S. S. Kumara, A. P. Senadeera, and R. M. M. Ruwanthika, "Development of sensorless based bimanual tele-rehabilitation robot for hemiparetic post-stroke patients," in *2024 Moratuwa Engineering Research Conference (MERCon)*, (Moratuwa, Sri Lanka), pp. 548–553, 2024.

[7] R. M. M. Ruwanthika, and S. Katsura, "Precise Slave-Side Force Control for Security Enhancement of Bilateral Motion Control during Application of Excessive Force by Operator," *Precision Engineering*, vol. 65, pp. 7–22, 2020.